Three-dimensional Statistical Modeling for Image Quality Improvements in Multi-Slice Helical CT

Jean-Baptiste Thibault, Ken Sauer, Charles Bouman, and Jiang Hsieh

***Abstract*— Multi-slice helical Computed Tomography (CT) scanning offers the advantages of faster acquisition and wide organ coverage for routine clinical diagnostic purposes. However, image reconstruction is faced with the challenges of three-dimensional cone-beam geometry, high pitches, and low dosage. Of all available reconstruction methods, statistical iterative reconstruction (IR) techniques appear particularly promising since they provide the flexibility of accurate physical noise modeling and geometric system description. In this paper, we present the application of Bayesian iterative algorithms to real 3D helical data to demonstrate significant image quality improvement over conventional techniques. Specifically, the reduction of helical cone-beam artifacts has been achieved, concurrently with enhanced image resolution and lower noise, as demonstrated by phantom studies. Clinical results also illustrate the noise reduction capabilities of the algorithm on real patient data. Although computational load remains a challenge for practical development, the superior image quality combined with the advancements in computing technology make IR techniques a legitimate candidate for future clinical applications.**

I. Introduction

Multi-slice CT scanning is particularly attractive for clinical applications due to short acquisition times, thin slices, and large organ coverage. Those acquisition trajectories produce projection measurements that pass obliquely through the 2-D reconstructed image planes. As the pitch increases, the deviation from conventional approximate two-dimensional planar data is further amplified. The accurate handling of this geometry is critical to the elimination of unwanted artifacts in the reconstructions and overall clinically acceptable image quality. Recent developments in analytical inversion algorithms give reason to hope that for many applications, image quality may be adequate under single-pass, deterministic inversion culminating in data backprojection. Imaging applications arise, however, in which characteristics of the scanner hardware places a limit on quality of reconstructions [1]. Helical streaks artifacts originate from portions of patient's anatomy, particularly in the case of abrupt edges in high-contrast materials, such as bones and prosthetics.

Jean-Baptiste Thibault is with the CT Reconstruction Group, GE Healthcare Technologies, 3000 N Grandview Bvd, W-1200, Waukesha, WI 53188. Telephone: (262) 312-7404. Email: jean-baptiste.thibault@med.ge.com

Ken Sauer is with the Department of Electrical Engineering, 275 Fitzpatrick, University of Notre Dame, Notre Dame, IN 46556-5637. Telephone: (574) 631-6999. Email: sauer@nd.edu

Charles Bouman is with the School of Electrical Engineering, Purdue University, West Lafayette, IN 47907-0501. Telephone: (765) 494-0340. Email: bouman@ecn.purdue.edu

Jiang Hsieh is with the Applied Science Laboratory, GE Healthcare Technologies, 3000 N Grandview Bvd, W-1200, Waukesha, WI 53188. Telephone: (262) 312-7635. Email: jiang.hsieh@med.ge.com

Traditionally, images have been reconstructed from CT data using so-called direct reconstruction algorithms such as filtered backprojection (FBP) or convolution backprojection (CBP). The FBP approach to image reconstruction from helical data that is currently used in commercial CT scanners relies heavily on helical view weighting interpolation schemes to account for helical geometry and thus address image artifacts [2]. However, approximations are intrinsic to any view data interpolation approach, and even with many refinements, CBP and other non-iterative variants are not likely ever to be able to completely resolve helical cone-beam artifacts. More complex techniques, such as the Feldkamp algorithm [3], attempt to address cone beam artifacts by doing three-dimensional filtered backprojection but do not consider the exact geometry of acquisition. The algorithms of Katsevich [4] provide an analytic solution to the helical cone beam scan inversion, but are derived under assumption of continuously sampled detector surfaces, not the discrete form necessary with hardware realizable in the foreseeable future.

As an attempt to provide more flexibility in the reconstruction choices, iterative reconstruction (IR) algorithms have been recently introduced for multi-slice helical CT images [5]. Although they typically imply a greater amount of computation than conventional methods, IR techniques offer the potential to produce images with significantly reduced artifacts. Rather than manipulating data to force it to conform to traditional direct reconstruction models, statistical methods attempt, to the degree possible, to *explicitly include non-idealities in the problem description*. This view of image reconstruction requires only that we have a description of the way in which each measurement is influenced by unknown image values. Errors and incompleteness in data are fully expected and their description built into the reconstruction process. Rather than treating all measurements with equal weighting, a statistical model allows differing degrees of credibility among data. This gives statistical methods a robustness not easily duplicated in backprojection techniques. Statistical methods offer flexibility in dealing with the various non-idealities in the data, as long as these can be accurately modeled.

Since the introduction of IR methods to CT, much of the effort has been devoted to demonstrating the feasibility of the proposed techniques and illustrating some of its benefits in the general case. The results in this paper focus on the performance of iterative reconstruction relative to the specific issue of helical cone-beam artifacts, while demonstrating lower noise at equivalent or greater resolution in all reconstructed images.

II. Statistical Model for Image Reconstruction

The objective of IR algorithms is to rely on successive operations of forward and backward projections in order to obtain the convergence of a derived optimization criterion describing the best match with the the measured projections. Let $\mathbf{y}$ be the measurement data, and let $\mathbf{x}$ be the unknown image to be reconstructed. In general, there will be a matrix $\mathbf{A}$ such that

$$E[\mathbf{y}] = \bar{\mathbf{y}} = \mathbf{A}\mathbf{x}$$

where $\bar{\mathbf{y}}$ is the noise free value of the measurement. The expression $E[\mathbf{y}]$ indicates the statistical average, or mean value, of the data $\mathbf{y}$. Statistical reconstruction methods generally work by finding a solution to the problem

$$\min_{\mathbf{x}} \left[\sum_i d_i (\mathbf{y}_i - [\mathbf{A}\mathbf{x}]_i)^2 + U(\mathbf{x}) \right], \tag{1}$$

where d_i may reflect the inherent variations in credibility of data, and $U(\mathbf{x})$ is a regularization term which encourages smoothness in the solution.

The crucial advantage of statistical reconstruction methods is that they allow any choice of the matrix $\mathbf{A}$. Any scanning geometry can be accurately modeled by proper computation of the entries in $\mathbf{A}$, regardless of the three-dimensional sampling. The model can be designed to be as close as possible to reality, although this may come at the cost of great computational expense. Because it is necessary to include the non-planar character of the measurements of the helical scan into the forward model, the computation of the elements of $\mathbf{A}$ must be done in the three spatial dimensions. This is a fundamental component to our approach. It requires software retracing of the slices of the scan during reconstruction in order to calculate the interaction between volumetric elements of reconstruction with X-rays at arbitrary angles in three dimensions. A crude but workable model involves the calculation of the intersection between scanner rays and voxels in the reconstruction space. An alternate technique with greater appeal in computation time and minimal loss in resolution involves resampling voxel and detector boundaries to calculate the contributions [6].

Because statistical reconstruction relies heavily on modeling of the "forward" process of data collection in the scanner, the greatest amount of effort must be applied to developing an accurate, yet manageable statistical description of the scanner's behavior. The elements d_i in quadratic form of (1) represent a measure of data credibility. For example, if a particular measurement y_i is photon-starved by some highly attenuating object, a problem which may cause artifacts in conventional images, by reducing the corresponding d_i, the statistical model reduces any error associated with that measurement.

The regularization term $U(x)$ enforces smoothness in the reconstructed images, independently of the formulation of the forward model. This penalty, normally extremely simple, is meant only to encourage the state in which neighboring entries in the image have similar values. Its parameters provide another level of control over the noise and resolution of the final image estimate. In order to account for interdependence of the neighboring planes in the three-dimensional acquisition volume, the formulation of the regularization must include all the neighbors of a given element in three-dimensional space. The Generalized Gaussian Markov Random Field (GGMRF) [7] has the desired effect and allows different level of edge-preservation by tuning the exponent parameter:

$$U(x) = \frac{1}{p\sigma^p} \sum_{\{j,k\} \in C} b_{j,k} |x_j - x_k|^p \tag{2}$$

C is the set of all neighboring pixel pairs in three-dimensions, and σ is a measure of the standard deviation of the noise in the measurements. Equation (2) ensures that sharp edges are increasingly well preserved as the exponent $1 \leq q \leq 2$ decreases, and maintains the desirable convex nature of the overall problem formulation.

III. Derivation of the Solution

The best optimization method to minimize the functional (1) is independent of the form of the estimator. Its choice must be based on its efficiency to reach the solution, while the final image is fully determined by (1). Statistical methods have a great advantage in the high-pitch multi-slice helical case, in having little dependence in their implementation on the geometry of data collection. We attack the estimation/optimization of (1) in the same manner regardless of the scan pattern represented by $\mathbf{A}$ or the selected prior $U(x)$. We propose to optimize over the full 3D volume through a sequence of one-dimensional updates where the image estimate $\hat{x}$ is

$$\hat{x} = \arg\min_{x \in \Omega} \left[\sum_i d_i \left(y_i - [Ax]_i \right)^2 + \frac{1}{q\sigma^q} \sum_{\{j,k\} \in C} b_{j,k} |x_j - x_k|^q \right]$$

and Ω is the convex set of positive reconstructions. This approach, called Iterative Coordinate Descent (ICD) [8], has shown rapid convergence properties provided a good choice of initial conditions, such as the FBP images. While the cost of each iteration remains high relative to FBP, a full 3D reconstruction typically converges in fewer than 20 iterations.

IV. Results

For this study, the reduction of helical streak artifacts has been a major goal of applying iterative techniques to CT. The various origins of these artifacts pose a significant difficulty for all algorithms. To illustrate this, we first selected a rib phantom scanned in 8x1.25mm collimation mode at helical pitch 13.4 on a Lightspeed scanner. The orientation of the Teflon ribs in three dimensions creates rapid variation of density in the z direction. Figure 1 illustrates how IR can remove nearly all the artifacts around the ribs caused by such variation. Greater accuracy in the forward model and some tuning of the prior parameters were necessary. Interestingly, IR techniques may also benefit more than FBP from increased spatial sampling of the reconstructions: simply by decreasing the size of the voxels, Figure 1 shows improvement in the resolution of rib details. In the FBP image, blurring of the ribs is evident when

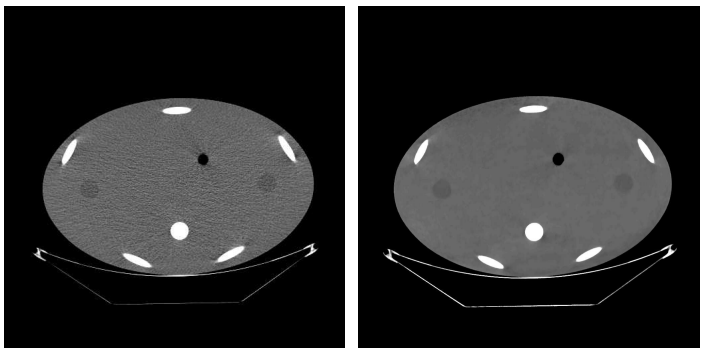

Fig. 1. Rib Phantom: 2D FBP (left) vs. Iterative (right), 8×1.25 Helical, Pitch 13.4, 320mA, 0.5 sec/rotation, WW=400; Iterative parameters: $\Delta x = \Delta y = 0.479$mm, $\Delta z = 0.625$mm, $q = 1.2$

compared to the better defined edges and smaller in-plane size of the ribs in the IR image.

In helical scans, IR is not inherently limited to spatial resolution matching the detector spacing, and gains in resolution are achievable beyond the limits of traditional methods like FBP by reconstructing smaller voxels. This is demonstrated more dramatically in Figure 2 from a 16x1.25mm scan of a head phantom at pitch 15. To further induce the artifact, the scan parameters were chosen beyond the recommended limits for clinical diagnostic scanning of this anatomy. The phantom itself, with the cracks in the skull varying rapidly from plane to plane, was also selected as a typical source of a high level of artifacts. The top-left image shows the artifact-free FBP for reference. In order to illustrate that the root cause of the artifact does not lie in geometric inaccuracies in the reconstruction method, we reconstructed the other images with major approaches proposed to tackle the multi-slice helical problem: a Feldkamp-based approach, Katsevitch's algorithm, and MAP-ICD. Even though all of them treat the exact geometry of acquisition with varying degrees of accuracy, the artifacts remain highly visible with all methods but IR. The IR images show better definition of the breaks in the bone which cause artifacts, as well as attenuating the streaks themselves. Appropriate prior modeling combined with increased spatial resolution through sub detector row width voxel sampling generates the benefit.

In addition to reducing helical cone-beam artifacts, the results in Figures 1 and 2 seem to qualitatively indicate the potential of IR methods to achieve greater resolution while significantly reducing the noise level in the reconstructed images. The gain in resolution/noise trade-off with iterative methods remains to be demonstrated by quantitatively comparing with conventional FBP. For this purpose, we considered the GE performance phantom scanned in 8x2.5mm helical mode at pitch 7 and 100mA. The wire section and resolution bars provide means to accurately measure the modulation transfer function (MTF), while the standard deviation of noise can be measured in the homogeneous regions of the phantom (water and plexiglass). The results are shown in Figure 3 and Table I. We compare both the standard kernel and the bone

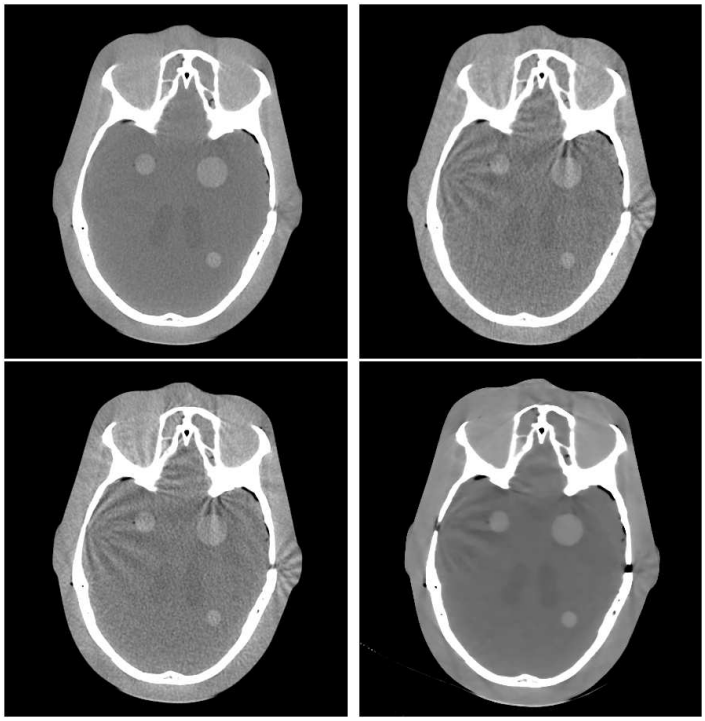

Fig. 2. Head Phantom: reference FBP (top left); Feldkamp-based (bottom left); Katsevich-based (top right); Iterative (bottom right); 16×1.25 Helical, Pitch 15.0, 320mA, 1 sec/rotation, WW=400; Iterative parameters: $\Delta x = \Delta y = 0.479$mm, $\Delta z = 0.625$mm, $q = 1.3$

	FBP Standard	FBP Bone	Iterative
50% MTF (line pair/cm)	4.18	8.79	8.95
10% MTF (line pair/cm)	6.92	13.02	14.84
Water Std. Dev.	12.54	66.67	2.69
Plexiglass Std. Dev.	12.02	77.33	1.95

TABLE I

COMPARISON OF FBP AND IR FOR MEASUREMENT OF MTF AND NOISE

kernel for conventional FBP to the IR images. The iterative reconstruction image may be regularized slightly too heavily, as witnessed by some loss of the fine resolution in the square hole at the lower left region of the bottom image of Figure 3. Nonetheless, the measured MTF is comparable to that of the FBP image reconstructed with bone kernel, while noise attenuation is 50% or more better in the IR image than in the FBP image with standard kernel.

Finally, the results of this study would not hold without successful application to real clinical data. For this, we selected a clinical head scan, in order to observe both soft tissue and bone. Figure 4 confirms that on clinical data as well, IR allows some improvements in resolution while dramatically reducing the noise level. Small structures present in the fat and soft tissue at the bottom of the head or the side of the orbits appear clearly in the IR image while they remain hidden by noise in the FBP images. The improvement in resolution is particularly visible around the sinus area, where the thin walls between the sinus cavities are clearly visible in the IR image.

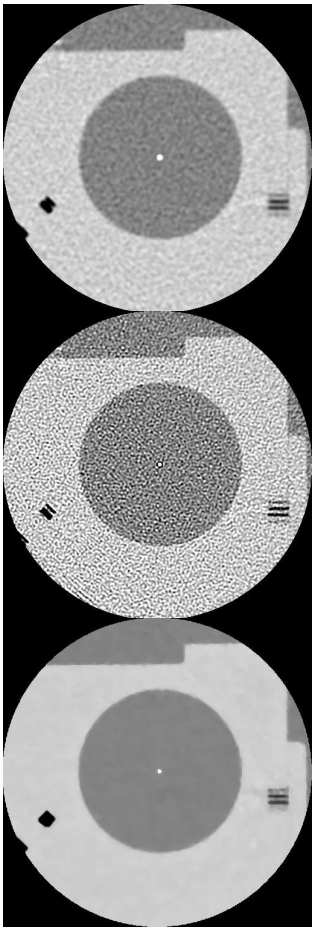

Fig. 3. Performance phantom: FBP standard kernel (top); FBP bone kernel (center); Iterative (bottom), 8 $\times$ 2.5 Helical, Pitch 7, 100mA, 1 sec/rotation, WW=400; Iterative parameters: $\Delta x = \Delta y = 0.122$mm, $\Delta z = 1.0$mm, $q = 1.1$

Meanwhile, the reduction of noise in the posterior fossa region allows better examination of the brain tissue. The fine detail in soft tissue is better preserved, but small variations in the bone are also compromised at a different window level. This points to some aspects of the non-Gaussian image model which may need to be adapted for better bone imaging.

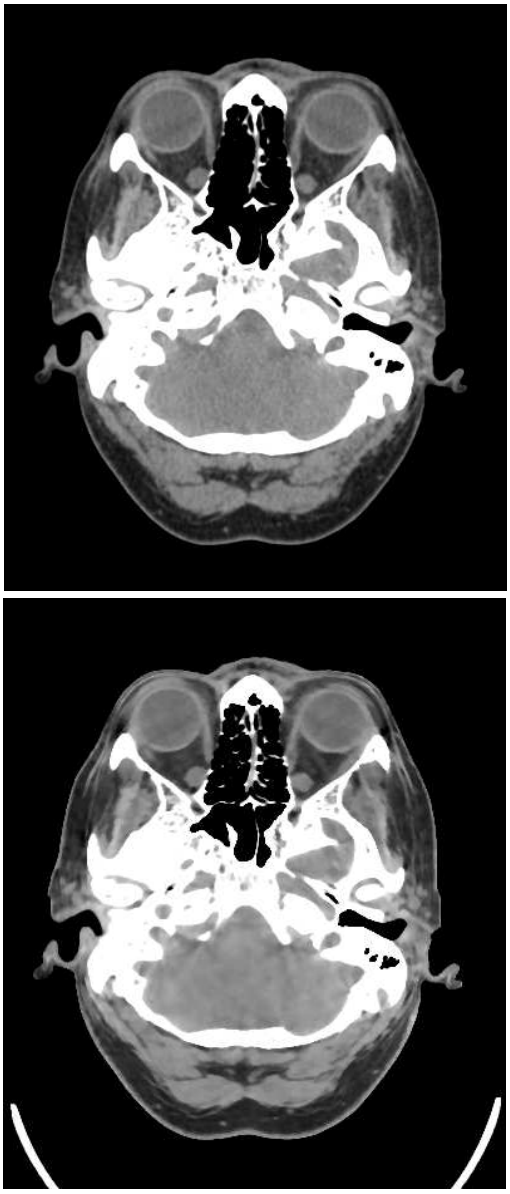

Fig. 4. Clinical Head: FBP (left) vs Iterative (right) 16 $\times$ 0.625 Axial, single slice reconstruction, WL=50, WW=400; Iterative recon params: $\Delta x = \Delta y =$0.479mm, $\Delta z =$0.625mm, $q =$1.3

V. Conclusion

We have presented a statistical framework for iterative image reconstruction for CT that produces very good image results. As the reconstruction technique remains independent from the exact form of the forward model, this method is applicable to any geometry, and particularly the multi-slice helical problem. Through appropriate selection of reconstruction parameters, iterative reconstruction achieves significant helical artifact reduction, at improved resolution and lower noise. Phantom results are confirmed on clinical data.

References

[1] M. Silver and K. Taguchi, "Windmill artifacts in multislice helical CT," in *Proc. of SPIE Conf. on Med. Imag.*, vol. 5032, May 2003, pp. 1918–1927.

[2] J. Hsieh, T. Toth, P. Simoni, B. Grekowicz, and G. Seidenschnur, "A generalized helical reconstruction algorithm for multi-slice CT," *Radiology 221(p)*, p. 217, 2001.

[3] L. A. Feldkamp, L. C. Davis, and J. W. Kress, "Practical cone-beam algorithm," *J. Opt. Soc. Am. A*, vol. 1, no. 6, pp. 612–619, 1984.

[4] A. Katsevich, "Analysis of an exact inversion algorithm for spiral cone-beam CT," *Phys. Med. Biol.*, vol. 47, pp. 2583–2597, 2002.

[5] J. Thibault, K. Sauer, C. Bouman, and J. Hsieh, "High quality iterative image reconstruction for multi-slice helical CT," in *Proc. Int. Conf. on Fully 3D Reconstruction in Rad. and Nuc. Med.*, June 29 - July 4 2003.

[6] B. Deman and S. Basu, "Distance-driven projection and backprojection in three-dimensions," *Phys. Med. Biol.*, vol. 49, pp. 2463–2475, 2004.

[7] C. A. Bouman and K. Sauer, "A generalized Gaussian image model for edge-preserving map estimation," *IEEE Trans. on Image Processing*, vol. 2, pp. 296–310, July 1993.

[8] K. Sauer and C. A. Bouman, "A local update strategy for iterative reconstruction from projections," *IEEE Trans. on Signal Processing*, vol. 41, no. 2, February 1993.